PROCEEDINGS OF SCIENCE

Bayesian Modeling of Galactic Cosmic-Ray Propagation

Ankit Yadav,[a,*] **Satyendra Thoudam,**[a] **Björn Eichmann**[b] **and Jörg P. Rachen**[c]

[a] *Department of Physics, Khalifa University of Science and Technology, PO Box 127788, Abu Dhabi, United Arab Emirates*

[b] *Institut für Theoretische Physik IV, Ruhr-Universität Bochum, Universitätsstrasse 150, 44780 Bochum, Germany*

[c] *Vrije Universiteit Brussel, Astrophysical Institute, Pleinlaan 2, 1050 Brussels, Belgium*

E-mail: 100062650@ku.ac.ae

Recent measurements from advanced cosmic-ray detectors have revealed spectral features that include a hardening in the GeV–TeV energy range, challenging the standard model of cosmic-ray acceleration and propagation. The re-acceleration of cosmic rays by weak shocks in the Galaxy offers a promising explanation, accounting for the observed spectral features of different nuclei and the boron-to-carbon (B/C) ratio. In this framework, cosmic rays are accelerated by strong supernova shocks before diffusing through the Galaxy. During propagation, they undergo re-acceleration upon encountering expanding supernova remnant shocks. Since older remnants are more likely to be encountered than younger ones due to their larger size, re-acceleration is predominantly driven by weaker shocks, resulting in a softer particle spectrum below ∼100 GeV. At higher energies, the spectrum is dominated by cosmic rays from young supernova remnants. In this study, we use the Markov Chain Monte Carlo (MCMC) method to determine key parameters governing cosmic-ray transport, such as diffusion properties, re-acceleration strength, and solar modulation, using observational data from the AMS-02, CALET, CREAM, DAMPE, and Voyager experiments. Preliminary results indicate that weak–shock re-acceleration can consistently reproduce the proton spectrum and the boron-to-carbon ratio.

39th International Cosmic Ray Conference (ICRC2025)
15–24 July 2025
Geneva, Switzerland

*Speaker

PoS(ICRC2025)154

1. Introduction

Understanding the origin and propagation of cosmic rays (CRs) is one of the most important open problems in astroparticle physics. Cosmic rays are primarily energetic, charged particles mainly protons and heavier nuclei that propagate through the interstellar medium and heliosphere before reaching the Earth's atmosphere. Their study provides valuable insights into high-energy astrophysical processes, magnetic turbulence in the interstellar medium, and potential cosmic-ray sources.

Over the past decade, high-precision measurements from instruments such as *AMS-02*, *ATIC-2*, *CALET*, *CREAM*, *DAMPE*, and *PAMELA* have revealed spectral features that deviate from the traditional expectation of simple power-law behavior. One of the most prominent features is the spectral hardening observed in the GeV–TeV energy range for both primary and secondary cosmic rays. In particular, the energy spectra of primary nuclei especially protons and helium exhibit hardening at rigidities around 200 GV [1–4]. Additionally, secondary-to-primary ratios, such as the boron-to-carbon (B/C) ratio, also display similar hardening features [5].

The observed spectral hardening in cosmic-ray nuclei at GeV–TeV energies challenges the standard model of cosmic-ray acceleration and transport, which typically assumes a single power-law source spectrum coupled with homogeneous, energy-dependent diffusion [6–9]. Several explanations have been proposed to account for these anomalies, including changes in the source injection spectra [10–13], spatial variations in the diffusion coefficient [14–16], and the influence of nearby sources [17–19].

Among these, the re-acceleration of cosmic rays by weak shocks from old supernova remnants (SNRs), as discussed in [20], provides a promising mechanism for explaining the hardening. In this model, cosmic rays that have been initially accelerated by strong SNR shocks may undergo further acceleration through interactions with weak, expanding shocks associated with older remnants in the interstellar medium. While this model reproduces the observed spectral hardening in the proton spectra, the corresponding propagation parameters do not fully account for the measured boron-to-carbon (B/C) ratio. In addition, constraints from low-energy observations, such as those provided by *Voyager-1*, were not included in the original analysis.

In this study, we revisit the weak shock re-acceleration scenario by performing a joint analysis of primary and secondary cosmic-ray data within a Bayesian inference framework. The objective is to determine a consistent set of propagation and re-acceleration parameters that can simultaneously account for the spectral hardening observed in protons and heavier nuclei, as well as the secondary-to-primary ratios such as B/C over a broad energy range. To improve agreement with the measured B/C ratio, we refine the model by introducing a break in the diffusion coefficient, motivated by recent observational findings [5]. High-precision measurements from *AMS-02*, *CREAM*, and *Voyager-1* are used to constrain the model parameters.

2. Re-acceleration Model

We follow the re-acceleration framework developed by Thoudam et al. (2014) [20], where cosmic rays (CRs) propagate through the Galaxy via spatial diffusion, undergo inelastic interactions, and are stochastically re-accelerated by repeated encounters with weak shocks in the interstellar

medium. These shocks are predominantly generated by old supernova remnants (SNRs), which are concentrated in the Galactic disk.

Cosmic rays are initially accelerated by strong shocks in young SNRs and injected into the interstellar medium. As they diffuse through the Galaxy, they may interact with older remnants that occupy larger volumes and are thus more likely to be encountered. Although these shocks are weaker, they can re-accelerate low-energy CRs to higher energies. This process introduces a softer secondary spectral component that is prominent at low energies, while at high energies the spectrum remains dominated by the original, non-reaccelerated population [21–23].

We model the CR propagation region as a cylinder with vertical boundaries at $z = \pm H$ and infinite radial extent. All sources and interactions are confined to an infinitely thin disk at $z = 0$ and radius R. Following Wandel et al (1987) [21], re-acceleration is incorporated as a secondary source term with a power-law momentum dependence. The steady-state transport equation for the differential number density $N(\vec{r}, p)$ is given by,

$$\underbrace{\nabla \cdot (D \nabla N)}_{\text{Diffusion}} - \underbrace{[\bar{n} v \sigma + \xi]\, \delta(z) N}_{\text{Losses (interaction + removal by re-acceleration)}} + \underbrace{\left[\xi s p^{-s} \int_{p_0}^{p} N(u)\, u^{s-1}\, du \right] \delta(z)}_{\text{Gain from re-acceleration}} = \underbrace{-Q\, \delta(z)}_{\text{Source term}}, \tag{1}$$

Here, $D(p)$ is the diffusion coefficient, $Q(p)$ the source spectrum, and ξ denotes the re-acceleration rate per unit volume. The quantities $\bar{n}$, $v(p)$, and $\sigma(p)$ represent the average surface density of interstellar matter, particle velocity, and the inelastic interaction cross-section, respectively. The $\delta(z)$ function confines all sources and interactions to the Galactic disk. The integral term represents the gain from particles re-accelerated from lower energies, and its shape is controlled by the re-acceleration index s. The re-acceleration rate is parameterized as $\xi = \eta V \bar{\nu}$, where $V = \frac{4\pi}{3} \mathcal{R}^3$ is the volume of a typical SNR with radius $\mathcal{R} = 100$ pc. The parameter η denotes the fraction of the volume effective for re-acceleration and is treated as a free parameter.

A low-momentum cutoff p_0 is introduced to exclude particles that are strongly affected by ionization and Coulomb losses. In contrast to earlier works where p_0 was fixed, we treat it as a free parameter that will be constrained in future analysis by comparing the ionization and Coulomb loss timescales [24] with the re-acceleration timescale.

The primary CR source term is modeled as

$$Q(r, p) = \bar{\nu}\, H(R - r)\, H(p - p_0)\, Q(p), \tag{2}$$

where $H(x)$ is the Heaviside step function, with $H(x) = 0$ for $x < 0$ and $H(x) = 1$ for $x > 0$. The radial extent of the source distribution is taken as $R = 20$ kpc. Each supernova is assumed to release a kinetic energy of $E_{\rm SN} = 10^{51}$ erg, and the average surface rate is taken as $\bar{\nu} = 25$ SNe Myr^{-1} kpc^{-2}, corresponding to about three supernova explosions per century in the Galaxy. The injected spectrum is parameterized as

$$Q(p) = A\, Q_0\, (Ap)^{-q}\, \exp\left(-\frac{Ap}{Z\, p_c} \right), \tag{3}$$

with A and Z the mass and charge numbers of the nucleus, q the source spectral index, Q_0 a normalization linked to the supernova energy budget, and $p_c = 10^7$ GeV taken as the high-momentum cutoff for protons.

The diffusion coefficient is modeled as a broken power law in rigidity,

$$D(p) = \begin{cases} D_0\beta \left(\frac{\rho}{\rho_0}\right)^{\delta_1}, & \rho < \rho_0, \\ D_0\beta \left(\frac{\rho}{\rho_0}\right)^{\delta_2}, & \rho \geq \rho_0, \end{cases} \tag{4}$$

where $\rho = Apc/(Ze)$ is the rigidity, $\beta = v/c$, and ρ_0 is the break rigidity.

Using Green's function techniques, the CR density at $r = 0$ and $z = 0$ is obtained as,

$$N(0,p) = \bar{v}R \int_0^\infty dk\, \frac{J_1(kR)}{L(p)} \Bigg\{ Q(p) + \xi s p^{-s} \int_{p_0}^{p} p'^{s}\, Q(p')\, \mathcal{A}(p') \exp\left[\xi s \int_p^{p'} \mathcal{A}(u)\, du\right] dp' \Bigg\} \tag{5}$$

where $L(p) = 2Dk\coth(kH) + \bar{n}v\sigma + \xi$ and $\mathcal{A}(p) = 1/(pL(p))$. J_1 is the Bessel function of the first kind of order one. The first term represents the direct component, while the second term accounts for the gain from re-acceleration.

Secondary CRs are modeled similarly, with the source term,

$$Q_2(r,p) = \bar{n}v_1(p)\sigma_{12}(p)H[R-r]H[p-p_0]N_1(r,p)\delta(z), \tag{6}$$

where $N_1(r,p)$ is the primary density. The secondary density at $r = 0$ is,

$$N_2(0,p) = R \int_0^\infty dk\, \frac{J_1(kR)}{L_2(p)} \Bigg\{ Q_2(0,p) + \xi s p^{-s} \int_{p_0}^{p} p'^{s} Q_2(0,p') \mathcal{A}_2(p') \exp\left[\xi s \int_p^{p'} \mathcal{A}_2(u)\, du\right] dp' \Bigg\} \tag{7}$$

with $L_2(p)$ and $\mathcal{A}_2(p)$ defined analogously.

The secondary-to-primary ratio is computed by taking the ratio of Eqs. (7) and (5) at fixed momentum. To account for solar modulation, we adopt the force-field approximation [25], treating the modulation potential $\Phi_{\rm SM}$ as a free parameter in the model.

Motivated by ongoing debate on the plasma environment just beyond the heliopause, We introduce a dimensionless constant parameter V_M that scales the LIS uniformly, written as $N_{\rm Voyager}(p) = V_M N_{\rm LIS}(p)$. While many works treat *Voyager-1* spectra as representative of the LIS [26], modeling and recent observations indicate a structured boundary layer with possible residual heliospheric influence outside the nominal heliopause [27–29], consistent with an energy-invariant normalization shift rather than a change of spectral shape [30]. Its expected value is unity; we adopt a prior centered at 1 and obtain posteriors for V_M, with deviations interpreted as indicators of boundary-layer effects, systematics etc.

3. Methodology

We constrain the key physical parameters governing Galactic cosmic-ray (CR) transport in a Bayesian framework using data from *AMS-02*, *CREAM*, and *Voyager-1*. The free parameters are

grouped by physical role: (i) diffusion ($D_0,\ \delta_1,\ \delta_2,\ \rho_0$); (ii) proton source ($q_p,\ f_p$) with $Q_0 \equiv f_p$; (iii) re-acceleration ($\eta,\ s$); (iv) solar modulation ($\Phi_{\rm P},\ \Phi_{\rm BC}$); and (v) Voyager modulation (V_M). Low-momentum cutoffs $p_{0,X}$ for protons, C, O, and B are also treated as free parameters for proof of concept, to be later determined from the comparison between loss processes and the re-acceleration timescale.

For this study, we adopt broad, independent uniform (flat) priors on all free parameters. The posterior follows Bayes' theorem,

$$P(\boldsymbol{\theta} \mid \mathcal{D}) \propto \mathcal{L}(\mathcal{D} \mid \boldsymbol{\theta})\, P(\boldsymbol{\theta}), \tag{8}$$

with Gaussian likelihoods under the assumption of independent measurement uncertainties. For a dataset with observed flux (or ratio) points $\{\mathrm{Obs}_i,\ \sigma_i\}$ and corresponding model predictions $\{\mathrm{Model}_i(\boldsymbol{\theta})\}$, we use

$$\mathcal{L}(\mathcal{D} \mid \boldsymbol{\theta}) \propto \exp\!\left[-\tfrac{1}{2}\,\chi^2(\boldsymbol{\theta})\right], \quad \chi^2(\boldsymbol{\theta}) = \sum_i \frac{\left[\mathrm{Model}_i(\boldsymbol{\theta}) - \mathrm{Obs}_i\right]^2}{\sigma_i^2}. \tag{9}$$

We first performed separate fits to the proton spectrum and to the B/C ratio. Given their close but not identical parameter estimates, our main analysis uses a joint fit in which primaries and secondaries are computed self-consistently. In the joint setup, the diffusion and re-acceleration parameters are shared across species, while the modulation potentials $\Phi_{\rm P}$ and $\Phi_{\rm BC}$ are allowed to differ. Following [20], the source spectral indices and normalizations for C and O are fixed to $q_{\rm C} = 2.24,\ f_{\rm C} = 0.024$ and $q_{\rm O} = 2.26,\ f_{\rm O} = 0.025$. The total likelihood can be written as,

$$\mathcal{L}_{\rm tot}(\boldsymbol{\theta}) = \mathcal{L}_{\rm P}(\boldsymbol{\theta})\, \mathcal{L}_{\rm BC}(\boldsymbol{\theta}). \tag{10}$$

Posterior sampling is performed with the affine-invariant ensemble sampler `emcee` [31]. We use 30 walkers initialized over a broad region of parameter space and a hybrid proposal scheme combining `emcee.moves.DEMove` (80%) and `emcee.moves.DESnookerMove` (20%), which provides a practical balance between global exploration and local refinement [32].

4. Results and Discussion

For this study, the inelastic interaction cross-section for protons is taken from Kelner et al. (2006) [33], and for heavier nuclei from Letaw et al. (1983) [34]. For boron secondaries, we adopt the production cross-sections from carbon and oxygen primaries as given by Heinbach & Simon (1995) [35]. The surface matter density is modeled as the average density in the Galactic disk within a distance equal to the half-height of the diffusion halo, H. We take $H = 5$ kpc, which gives an average atomic hydrogen surface density of $\bar{n} = 7.24 \times 10^{20}$ atoms cm^{-2} [20]. An additional 10% is included to account for helium in the interstellar medium.

Figure 1 shows that weak–shock re-acceleration provides a consistent description of both the proton spectrum and the boron–to–carbon ratio using a *single* transport parameter set (Table 1). The residuals, expressed as (data − model)/model, demonstrate satisfactory agreement across the fitted energy range. A detailed discussion on how re-acceleration qualitatively modifies primary and secondary spectra can be found in Thoudam et al. (2014) [20].

Table 1: Posterior medians and 1σ HDIs (16%–84%) with best-fit ("maximum likelihood"). Here, HDI denotes the highest density interval, i.e. the narrowest interval containing 68% of the posterior probability. Subscripts: $\Phi_{\rm BC}$ is the modulation potential for the B/C ratio, $\Phi_{\rm P}$ for protons, and $p_{0,X}$ denotes the low-momentum cutoff for species X. All momenta are per nucleon.

Parameter	**Median**	**HDI 16%**	**HDI 84%**	**Best-fit**
Diffusion				
δ_1	0.11	−0.10	0.38	0.08
δ_2	0.27	0.25	0.28	0.25
ρ_0 [GV]	1.06	0.68	1.28	0.78
D_0 [cm^2 s^{-1}]	5.02×10^{28}	4.47×10^{28}	5.64×10^{28}	5.40×10^{28}
Primary source (for proton spectrum)				
q_p	2.32	2.31	2.33	2.32
$f_{\rm P}$ [$\times 10^{49}$ erg]	4.33	4.25	4.43	4.35
Re-acceleration				
η	0.78	0.70	0.88	0.91
s	4.94	4.76	5.11	5.00
Solar modulation				
$\Phi_{\rm BC}$ [MV]	643.00	555.00	780.00	640.00
$\Phi_{\rm P}$ [MV]	635.00	631.00	645.00	640.00
Voyager				
V_M	1.02	0.91	1.85	1.03
p_0 *from Eq. 1*				
$p_{0,\rm P}$ [MeV/c]	449.00	411.00	483.00	421.00
$p_{0,\rm C}$ [MeV/c]	912.00	849.00	972.00	838.00
$p_{0,\rm O}$ [MeV/c]	151.00	137.00	157.00	137.00
$p_{0,\rm B}$ [MeV/c]	561.00	195.00	665.00	467.00

At low energies, the LIS comparison with Voyager data is particularly sensitive to the choice of low–momentum cutoff p_0. For carbon, the posterior median is $p_{0,\rm C} = 912$ MeV/c (corresponding to ~ 320 MeV/n), with a 1σ HDI of 849–972 MeV/c (kinetic energy range $\sim$ 298–341 MeV/n). To remain within the validity of the model, the χ^2 evaluation is restricted to energies above the largest p_0 among the species, so not all Voyager points are included in the likelihood evaluations for MCMC.

In the next stage, the low–momentum cutoffs will no longer be left as free parameters. Instead, for each species they will be determined by comparing the weak–shock re-acceleration timescale with ionization and Coulomb loss timescales, controlled through the re-acceleration–timescale parameter. This procedure is expected to regularize the low–energy LIS behavior and extend the comparison with Voyager data to lower energies, while maintaining a unified description of primaries and the B/C ratio within the same Bayesian framework.

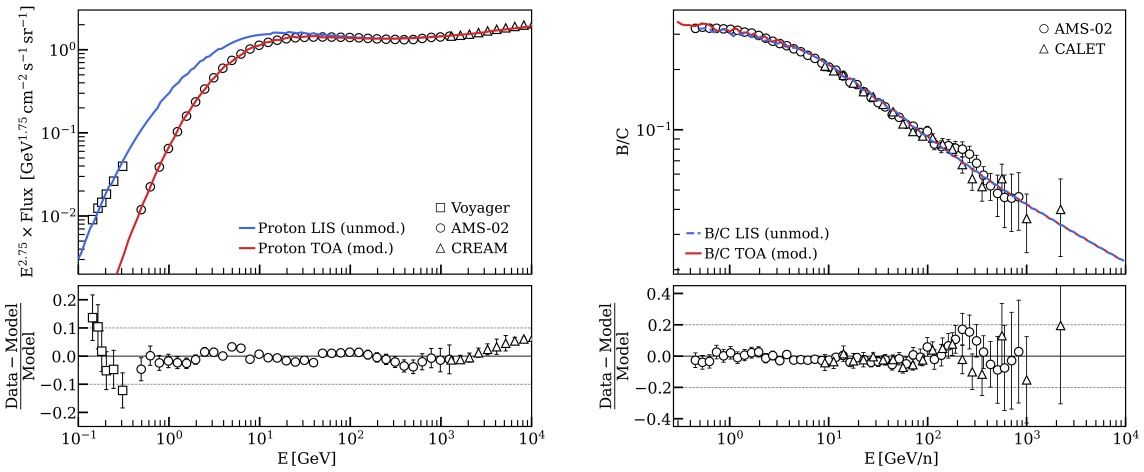

(a) Proton spectrum

(b) Boron-to-carbon ratio

Figure 1: Joint best-fit model for (a) protons and (b) the B/C ratio using a single transport parameter set (Table 1). Blue curves show the unmodulated local interstellar spectra (LIS), while red curves include solar modulation to top-of-atmosphere (TOA). Residual panels display the fractional difference (data − model)/model, with gray dashed lines as visual guides.

5. Conclusion

The present analysis demonstrates that weak–shock re-acceleration can simultaneously reproduce the proton flux and the boron–to–carbon ratio within a single Bayesian framework, providing a unified description of primaries and secondaries.

Future work will extend this framework to heavier nuclei, where their source and transport parameters can be constrained directly by the observed data. In addition, the low–momentum cutoffs p_0 will be derived self-consistently from the balance between re-acceleration and loss timescales, leading to a more robust description of re-acceleration across Galactic cosmic-ray nuclei.

References

[1] A. D. Panov, J. H. Adams, H. S. Ahn, and et al. *Bull. Russ. Acad. Sci. Phys.*, 73:564, 2009.

[2] O. Adriani, G. C. Barbarino, G. A. Bazilevskaya, and et al. *Science*, 332:69, 2011.

[3] Y. S. Yoon, H. S. Ahn, P. S. Allison, and et al. *ApJ*, 728:122, 2011.

[4] M. Aguilar, L. Ali Cavasonza, G. Ambrosi, and et al. *Phys. Rep.*, 894:1, 2021.

[5] DAMPE Collaboration. *Sci. Bull.*, 67:2162, 2022.

[6] G. F. Krymskii. *Akad. Nauk SSSR Dokl.*, 234:1306, 1977.

[7] A. R. Bell. *MNRAS*, 182:147, 1978.

[8] R. Blandford and D. Eichler. *ApJ*, 221:L29, 1978.

[9] V. L. Ginzburg and V. S. Ptuskin. *RvMP*, 48:161, 1976.

[10] P. L. Biermann, J. K. Becker, J. Dreyer, and et al. *ApJ*, 725:184, 2010.

[11] Y. Ohira, K. Murase, and R. Yamazaki. *MNRAS*, 410:1577, 2011.

[12] Q. Yuan, B. Zhang, and X.-J. Bi. *PRD*, 84:043002, 2011.

[13] V. S. Ptuskin, V. Zirakashvili, and E. S. Seo. *ApJ*, 763:47, 2013.

[14] N. Tomassetti. *ApJL*, 752:L13, 2012.

[15] P. Blasi, E. Amato, and P. D. Serpico. *PRL*, 109:061101, 2012.

[16] R. Aloisio and P. Blasi. *JCAP*, 07:001, 2013.

[17] S. Thoudam and J. R. Hörandel. *MNRAS*, 421:1209, 2012.

[18] A. D. Erlykin and A. W. Wolfendale. *Astropart. Phys.*, 35:449, 2012.

[19] G. Bernard, T. Delahaye, Y.-Y. Keum, and et al. *A&A*, 555:A48, 2013.

[20] S. Thoudam and J. R. Hörandel. *A&A*, 567:A33, 2014.

[21] A. Wandel, D. S. Eichler, J. R. Letaw, R. Silberberg, and C. H. Tsao. *ApJ*, 316:676, 1987.

[22] E. G. Berezhko, L. T. Ksenofontov, V. S. Ptuskin, V. N. Zirakashvili, and H. J. Völk. *A&A*, 410:189, 2003.

[23] V. Ptuskin, V. Zirakashvili, and E. Seo. *Proc. ICRC*, 2011.

[24] A. W. Strong and I. V. Moskalenko. *ApJ*, 509:212, 1998.

[25] L. J. Gleeson and W. I. Axford. *ApJ*, 154:1011, 1968.

[26] A. C. Cummings, E. C. Stone, B. C. Heikkila, and et al. *ApJ*, 831:18, 2016.

[27] M. Zhang, X. Luo, and N. Pogorelov. *Phys. Plasmas*, 22:091501, 2015.

[28] N. V. Pogorelov, J. Heerikhuisen, V. Roytershteyn, and et al. *ApJ*, 845:9, 2017.

[29] D. L. Turner, A. Michael, E. Provornikova, and et al. *ApJ*, 960:130, 2024.

[30] N. A. Schwadron and D. J. McComas. *ApJL*, 778:L33, 2013.

[31] D. Foreman-Mackey, D. W. Hogg, D. Lang, and J. Goodman. *PASP*, 125:306, 2013.

[32] D. Foreman-Mackey, W. Farr, M. Sinha, and et al. *JOSS*, 4:1864, 2019.

[33] S. R. Kelner, F. A. Aharonian, and V. V. Bugayov. *PRD*, 74:034018, 2006.

[34] J. R. Letaw, R. Silberberg, and C. H. Tsao. *ApJS*, 51:271, 1983.

[35] U. Heinbach and M. Simon. *ApJ*, 441:209, 1995.